Active Magnetic Bearing for Tubular Linear Induction Motor Applied to Onshore Oil Exploitation*

Eduardo Alves da Costa[1,a], Ivan Eduardo Chabu[2,b], Jose Jaime da Cruz[2,c]
[1]Federal Institute of Education, Science and Technology of São Paulo, 01109-010, Brazil
[2]Polytechnic School, University of São Paulo, São Paulo, 05508-900, Brazil
[a]educosta@uol.com.br, [b]ichabu@pea.usp.br, [c]jaime@lac.usp.br

Abstract: A tubular linear induction motor applied to onshore oil exploitation was proposed recently. Its purpose is to directly drive the sucker-rod pump installed in the down hole of the oil well. In continuing the research an active magnetic bearing (AMB) was developed and applied to the motor in substitution to the existing mechanical bearing. Instead of the usual eight-pole AMB, a different concept is adopted where a DC-excited primitive bearingless machine is used as a magnetic bearing. The magnetic bearing levitation control is executed by a digital controller using an AD/DA converter and a control algorithm implemented in FPGA hardware. A linear model is written to describe its dynamics. In this work the AMB system is studied with particular emphasis to the experimental results obtained with the prototype in operation. Tests performed on this prototype show that the AMB can be an interesting alternative to be considered in this context.

Keywords: Active Magnetic Bearing, Linear Induction Motor, Bearingless Motor, Feedback Control System, Oil Pump

Introduction

The onshore oil exploitation is traditionally done by walking beam systems as shown in Fig. 1a. Problems with the flexible parts and rupture of the rod frequently occurs taking to long stops for maintenance. The use of this equipment can be limited depending on the depth and non straight form of the oil well.

A novel approach to onshore oil pumping has been proposed recently [1]. A prototype of a Tubular Linear Induction Motor (TLIM) applied to onshore oil exploitation, named MATÆOS (which is in the Portuguese acronym for Tubular Asynchronous Motor for Onshore Oil Exploitation) was built by the Applied Electromagnetism Laboratory (LMAG) of the University of São Paulo [2]. Its aim is to directly drive the onshore downhole piston pump with no use of rods (see Fig. 1b). This kind of application is new and the motor is intended to replace the mechanical surface system and the rod string with advantages: it is a simpler system that requires less maintenance, has lower production costs and higher reliability. Being modular the MATÆOS can be configured to drive different pumps and to operate at wide range of depths by just connecting an appropriate number of its modules.

With the increasingly development of technology, Active Magnetic Bearing (AMB) systems have been applied in the last years in several areas, such as vacuum pumps, centrifuges, blood pumps, energy storage flywheels and semiconductor processes [3,4,5]. Thus, the AMB arises as an interesting alternative to support the MATÆOS shaft (secondary) in view of the numerous advantages over conventional bearings, such as absence of mechanical contact, lower losses caused by axial motion, no need of lubrification, active vibration control, longer life and less maintenance requirements. The later is particularly true

* This work is supported by Fapesp under Grant No. 2008/01900-7. The third author is also grateful to CNPq.

in the oil exploitation application, where the fluid is abrasive and can rapidly damage the mechanical bearing.

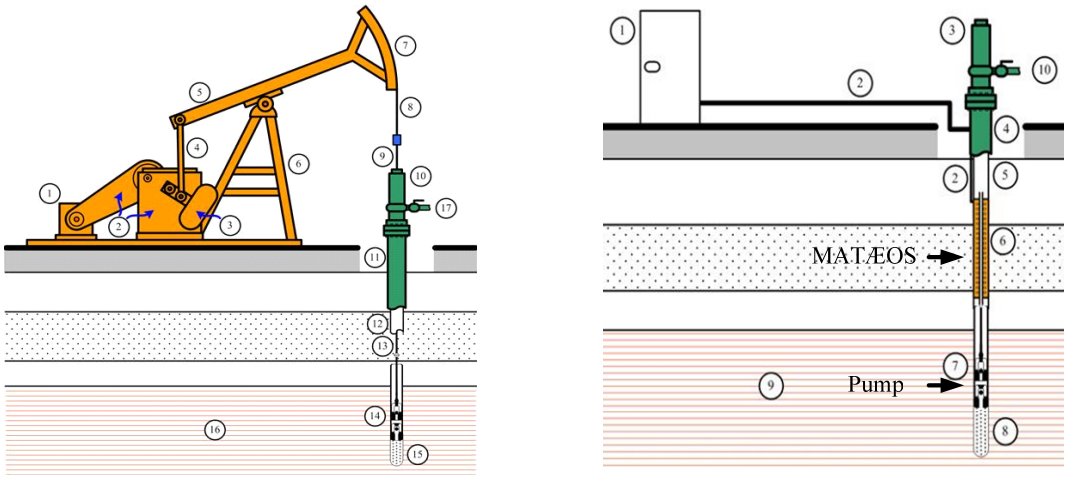

(a) Walking beam system. (b) Oil pumping system with MATÆOS.

Fig. 1 Comparative scheme of onshore oil exploitation systems.

In continuation of the research accomplished at the University of São Paulo concerning magnetic levitation systems, an AMB [6] has been developed and applied to the prototype of the TLIM in substitution to the existing mechanical bearing. The scope of the project covers the design, construction and testing of the AMB prototype including the mechanical, electrical and software components required to the operation of the system. Usually AMBs have eight magnetic poles [4]. A different choice has been made here with a DC-excited primitive bearingless (self-bearing) machine [5]. As in the conventional radial magnetic bearing, a DC current was used to excite the motor windings in order to generate a static 4-pole bias flux distribution; the other set of 3-phase windings connected to a 3-phase inverter have been used as a suspension winding. Since the AMB is intended to operate at the well bottom, this choice has a direct impact on the system reliability in view of the smaller numbers of power devices and connection wires required [6].

The electromagnet design was accomplished using the Finite Element Method (FEM) in the analysis of both the flux density and the relationship between the radial force and the suspension winding current. Sensors were located on the stator x- and y-axes to measure the secondary radial displacement. The power amplifier was a 3-phase intelligent switching chip that received the Pulse Width Modulation (PWM) signals generated by the digital control system and supplied the current for each phase. The magnetic bearing levitation control was performed by a real-time digital controller using an AD/DA converter and a control algorithm that ran in a Field Point Programmable Array (FPGA) hardware using the Labview graphical language.

This paper focuses on the design, construction and testing of such AMB system with particular emphasis to the experimental results obtained with the prototype in operation.

AMB Radial Force Generation

The most common 8-pole AMB configuration with radial force generation in the direction of the *x*-axis is shown in Fig. 2a. The eight poles are divided into four electromagnets but only

windings 1 and 3 are shown. Denoting the current on winding *i* by I_i then if $I_1 > I_3$ the magnets generate a resultant radial force (*F*) in *x*-axis direction. The AMB model can be linearized with magnets operating in differential driving mode using bias current. In total, eight wires are necessary for connection between the radial magnetic bearing and the four current drives.

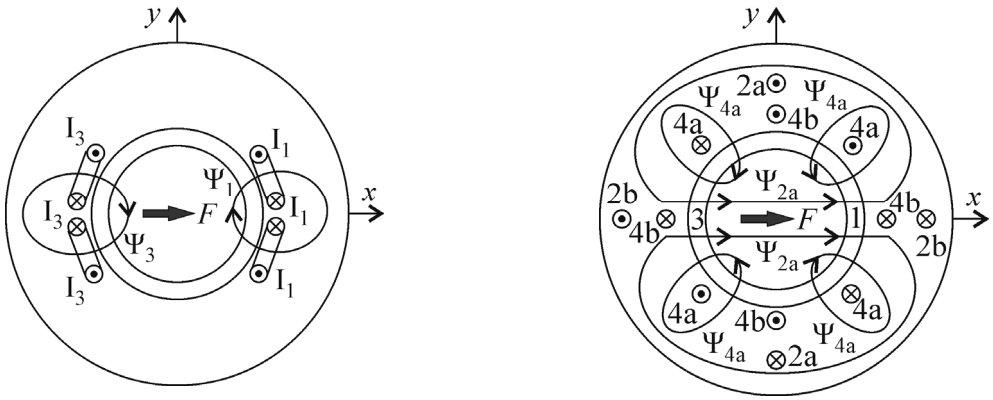

(a) 8-pole AMB with $I_1 > I_3$.

(b) DC-excited primitive bearingless machine.

Fig. 2 Comparative scheme to *x*-axis direction.

Fig. 2b shows the cross section of a DC-excited primitive bearingless machine in the case where the resultant radial force (*F*) in the *x*-axis direction is generated assuming that the currents are set to zero in both 2*b* and 4*b* windings. Two sets of windings are wound in the stator. One of them is a 4-pole torque winding (4*a*) and the other one is a 2-pole radial force winding (2*a*). In this project the bearingless machine does not have the purpose of torque generation, being the DC current used just to excite the torque winding. When the shaft (TLIM secondary) is centered with respect to the stator and there is no current in the suspension winding, a symmetrical 4-pole flux Ψ_{4a} will be produced and the flux density at each air gap will be the same. If a disturbance displacement of the shaft occurs towards the negative direction of the *x*-axis, the symmetrical flux distribution in the shaft air gap will be broken. In order to bring the shaft back to the central position the current of the suspension winding must be controlled. If the coil 2*a* carries a positive current as shown in Fig. 2b, a 2-pole flux wave Ψ_{2a} is generated. Then, the flux density in air gap 1 is increased whereas the flux density in air gap 3 is decreased. Thus, a positive radial force *F* is produced in order to draw the shaft back to the center. A radial force in the negative direction of *x*-axis can be generated with a negative current in 2*a* windings. Similarly, the radial forces in *y*-axis can be produced by controlling the current of windings 2*b*. Consequently, a radial force is generated by the interaction of the 4-pole static magnetic field and the suspension winding currents.

Although for the sake of simplicity just 2-phase windings are described, in this work a 3-phase radial magnetic bearing was constructed.

The following assumptions are made: the magneto-motive force can be well approximated by its first harmonic, the magnetic circuit is linear, iron permeability is infinite, eccentric rotor displacement is small with respect to the air gap length and primitive bearingless machine is used only as a radial magnetic bearing (a DC current of value I_4 excites the motor winding i_{4a} and i_{4b} is set as zero). The suspension forces F_x and F_y, respectively in *x* and *y* directions of the bearingless machine, shown in Fig. 2b, can then be written as [5]:

$$\begin{bmatrix} F_x \\ F_y \end{bmatrix} = M' I_4 \begin{bmatrix} i_{2a} \\ -i_{2b} \end{bmatrix}. \tag{1}$$

The currents i_{2a} and i_{2b} are, respectively, instantaneous currents of windings 2*a* and 2*b*. *M'* is the derivative of the mutual inductance with respect to the secondary radial displacements *x* and *y*, that represents the coupling between the 4-pole and the 2-pole windings. *M'* can be written approximately as:

$$M' = \frac{\pi \mu_0 R l N_2 N_4}{8 g_0^2} \tag{2}$$

where μ_0 is the permeability of vacuum, R is the secondary radius, l is the axial length, N_2 and N_4 are, respectively, the numbers of turns of the 2-pole and 4-pole windings and g_0 is the nominal air gap length.

The value of *M'* can also be measured experimentally [5].

The suspension forces evaluated by Eq. (1) allowed electromagnet design and the first time levitation of TLIM secondary. Nevertheless, a better approximation to AMB forces F_x and F_y can be written as [4]:

$$\begin{cases} F_x = k_i i_{2a} + k_s x \\ F_y = -k_i i_{2b} + k_s y \end{cases} \tag{3}$$

where k_i and k_s are, respectively, force-current and force-displacement constants.

Since the closed-loop is available, for experimentation, the values of both k_i and k_s were gotten experimentally by applying known loads in the secondary and imposing an offset on the radial position.

System Configuration

A sketch of the cross section of the TLIM with two magnetic bearings is shown in Fig. 3. Presently one of them is electromagnetic and the other one is mechanical. The TLIM has a modular construction which allows the adjustment of its total thrust to the force required to lift the oil column from the bottom of the well to the ground surface. The secondary of the TLIM levitates under the action of the radial electromagnetic bearing. Furthermore there are retainer bearings to prevent the secondary from touching down the primary when the AMBs fail to work during operation. They also protect the secondary when dynamical loads exceed the AMB load-carrying capacity.

The radial bearing is fixed to the primary of the motor. This bearing is a DC-excited primitive bearingless 3-phase machine with two sets of windings. The values of the main parameters of both the AMB and the TLIM are listed in Table 1.

A view of the system with the TLIM prototype and main hardware of the AMB is shown in Fig. 4.

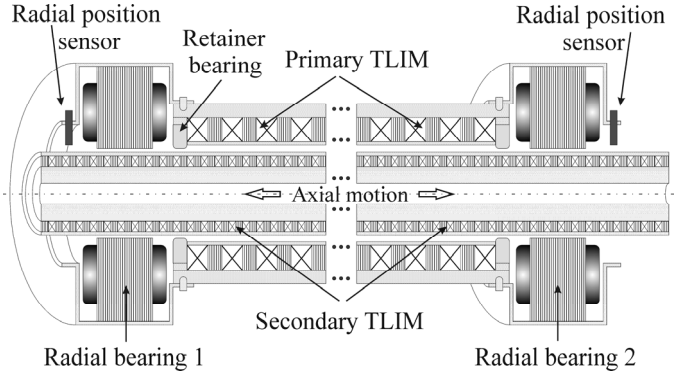

Fig. 3 Cross section of motor with electromagnetic bearings.

Table 1 Parameters of both the TLIM and the AMB.

Tubular linear induction motor	
Stator outer diameter	124 [mm]
Length (one module)	750 [mm]
Synchronous Velocity	1.5 [m/s]
Secondary outer diameter (shaft)	60.1 [mm]
Secondary length	2400 [mm]
Air gap length	1.75 [mm]
Secondary (shaft) weight	45.6 [kg]
AMB	
Inner / Outer diameter of the stator	62.5 / 170 [mm]
Radial air gap length	1.2 [mm]
Axial length	140 [mm]
Number of phases	3

Position Sensor. The secondary of the TLIM is made of carbon steel with a copper ring cage. Both are covered with a carbon steel coat. Inductive sensors have been chosen to measure the AMB air gaps in two orthogonal directions. Two sensors were used for each one of them. Despite the non-homogeneity of the secondary the tests performed showed that the sensor static characteristic was linear. The sensor has a sensitivity of 2.5V/mm, a resolution of 1μm and a switching frequency of 1.6kHz.

Power Amplifier. It is a 3-phase intelligent switching amplifier SA305 from Apex Microtechnology Corp. with three independent half bridges which can provide up to 5A DC and 10A of peak per 200ms. The power amplifier receives the PWM signals generated by the digital control system and supplies the current to each phase of the suspension windings i_{2u}, i_{2v} and i_{2w}.

Electromagnet. Using finite element analysis the electromagnet was designed [6,7]. Simulation was conducted based on both the drawing of a model with the magnetic flux density and the relationship between the radial force and the suspension winding current. In accordance with a principle of bearingless motor design [5] the numbers of poles of the torque windings and of the control winding must differ by two. This means that the windings must be at least 2- and 4-pole ones. Hence in the 3-phase system the minimum number of stator teeth must be 12, which is the number of slots used in this project. Fig.5 shows both the 4-pole (4*u*, 4*v*, 4*w*) and 2-pole (2*u*, 2*v*, 2*w*) winding sets arrangements.

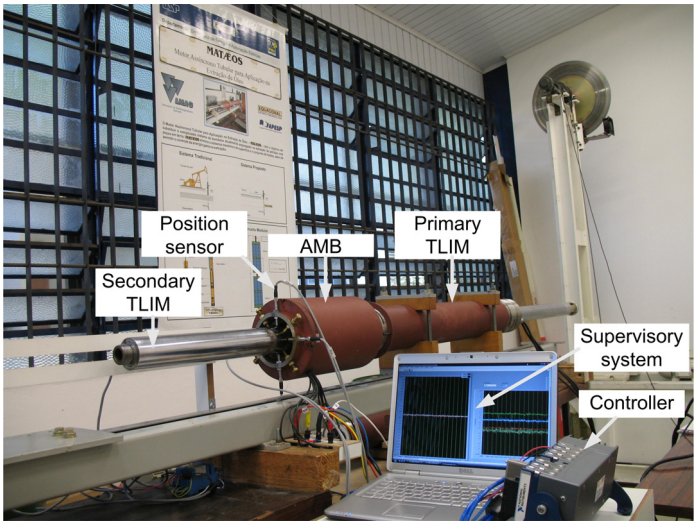

Fig. 4 View of the TLIM prototype with AMB hardware.

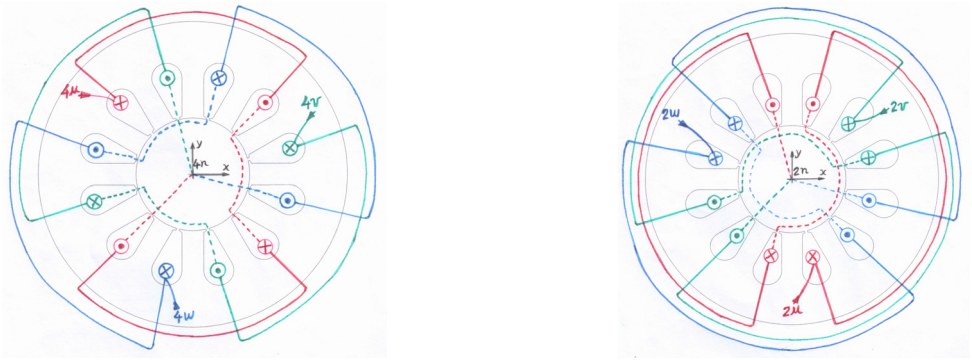

(a) 4-pole winding. (b) 2-pole suspension winding.

Fig. 5 Three-phase winding sets arrangement.

AMB Control System. The controller structure (see Fig. 6) is of the cascade type having a position primary loop and a current secondary loop. Position sensor measurements from axes x and y are compared, respectively, to their reference values x^* and y^*, typically null. The errors are input to position controllers which compute the two-phase currents i_{2a}^* and i_{2b}^*. The three-phase currents commands i_{2u}^*, i_{2v}^* and i_{2w}^* are evaluated by using the inverse Clark transform. These currents are the reference ones for the current loops which are fed back with the actual measured ones i_{2u}, i_{2v} and i_{2w}, respectively. The errors are input to current controllers and in the PWM block the control signals H_A, L_A, H_B, L_B, H_C and L_C are generated and used to switch the power amplifier. The torque windings are driven by a DC current I_4 that produces a static 4-pole flux distribution or bias flux.

The control system hardware includes analog input and digital output modules as well as a FPGA device to carry out the real-time digital control with high performance. The hardware is complemented by a control application developed in Labview graphical language. The current controller has been implemented in the form of an on-off control with a 100kHz sampling rate. The primary loop for radial displacement control was performed by an usual PID controller with a high-pass filter operating at a 12.5kHz sampling rate.

Nevertheless the control of the AMB has some practical problems. The longitudinal motion of the motor secondary generates radial disturbances in the AMB, making thus the control difficult. The mass supported by the magnetic bearing varies during the motion cycle of the TLIM. Additionally the parameter that relates the electromagnetic force caused by the radial displacement of the secondary from the center of the TLIM primary has a significant uncertainty. In view of these characteristics robustness arises as a natural requirement in the design of the position controller. Using classical control tools a robust controller has been designed in order to comply with the specifications [7].

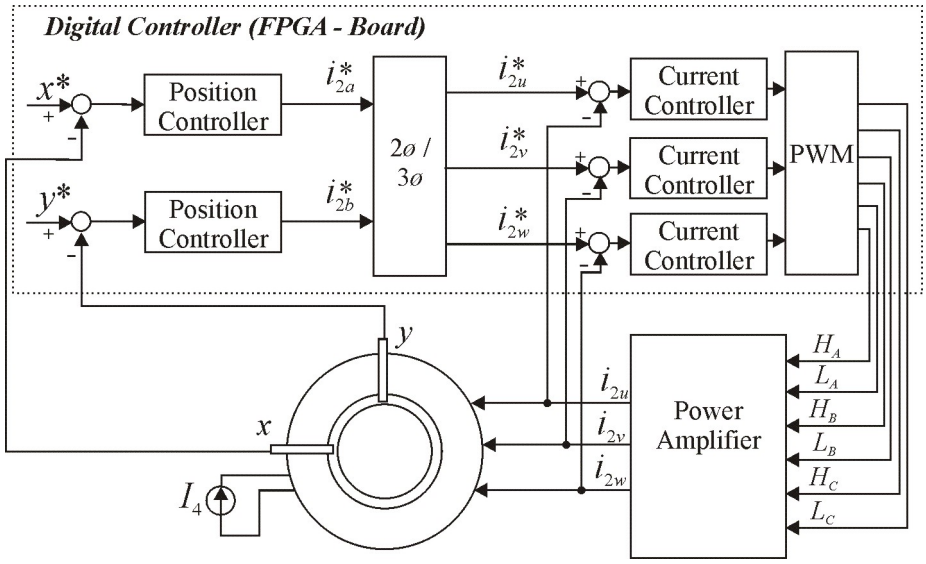

Fig. 6 Block diagram for closed-loop operation.

Mathematical Model

Figure 7 shows the forces acting on the TLIM secondary with two radial magnetic bearings.

From the second Newton´s law the following equations can be written:

$$\begin{cases} m\ddot{x}_1 = F_{x1} + F_{mx1} + d_{x1} \\ m\ddot{y}_1 = F_{y1} + F_{my1} + d_{y1} - mg \\ m\ddot{x}_2 = F_{x2} + F_{mx2} + d_{x2} \\ m\ddot{y}_2 = F_{y2} + F_{my2} + d_{y2} - mg \end{cases} \tag{4}$$

where m is the mass of half secondary of the TLIM; g is the local gravity acceleration; x_1, y_1, x_2 and y_2 are secondary displacement from the center of the TLIM primary and AMB stator, respectively, along x_1, y_1, x_2 and y_2-axis directions; F_{x1} and F_{y1} are the components of the radial force generated by the magnetic bearing 1 along x_1 and y_1-axis directions, respectively; F_{x2} and F_{y2} are similarly defined; F_{mx1}, F_{my1}, F_{mx2} and F_{my2} are the components of the external disturbance generated by the motor due secondary displacement from the center of the TLIM primary along x_1, y_1, x_2 and y_2-axis directions, respectively; d_{x1}, d_{y1}, d_{x2} and d_{y2} are the components of the disturbance produced by gravity, respectively, along x_1, y_1, x_2 and y_2-axis directions, due to the longitudinal motion of the TLIM secondary.

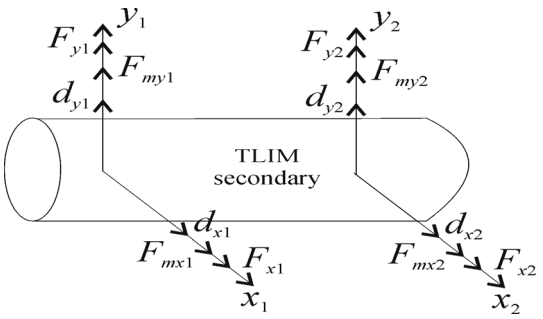

Fig. 7 Scheme of forces acting on the TLIM secondary.

Since the TLIM prototype has presently only one electromagnetic bearing, being the other one mechanical, then the subscripts $_1$ and $_2$ will be omitted in Eq. (4).

F_x and F_y are control forces whereas F_{mx}, F_{my}, d_x and d_y are disturbance forces. Assuming a constant speed longitudinal motion of the secondary, during each half-cycle d_y can be considered as a ramp (actually, it is a triangle waveform) since then the corresponding weight supported by AMB increases linearly with time. For small values of x and y, a linear relationship can be assumed:

$$\begin{cases} F_{mx} = k_m x \\ F_{my} = k_m y \end{cases} \tag{5}$$

where k_m is a force-current constant.

As usual, the Laplace transform of a function $f(t)$ is denoted by $F(s)$. For y expressed in millimeters, the block diagram of the closed-loop control system corresponding to the y axis is given in Fig. 8, where $G_c(s)$ is the position controller transfer function,

$$G_p(s) = \frac{1000}{ms^2} \tag{6}$$

is the plant transfer function and

$$G_i(s) = \frac{250}{s + 250} \tag{7}$$

is the transfer function of the current loop.

From the block diagram it follows immediately that

$$Y(s) = \frac{1000[-k_i I_{2b}(s) - mgD(s) + D_y(s)]}{ms^2 - 1000(k_s + k_m)}. \tag{8}$$

Therefore the open-loop system is unstable since it has one positive real pole.

The following nominal values were obtained for the AMB prototype: m=22.8kg, k_s=270N/mm, k_i=164N/A, k_m=308N/mm.

Motion along x-axis has a model identical to the y-axis one, except that now the gravity effect is absent.

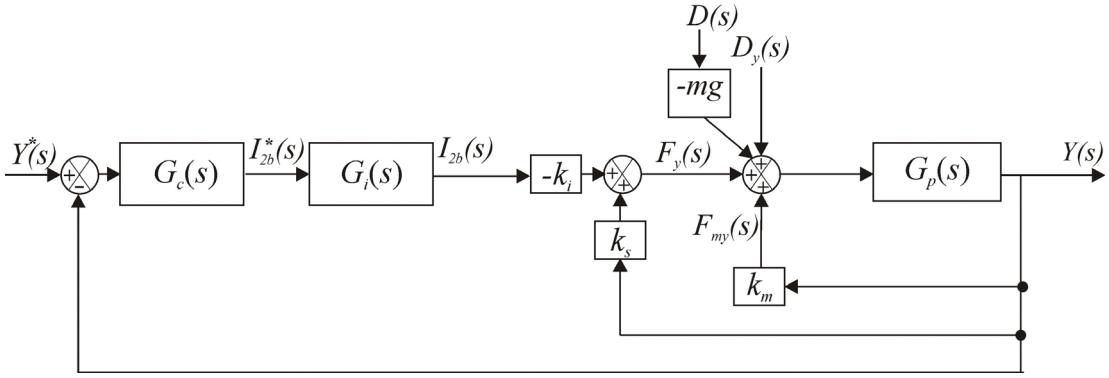

Fig. 8 Block diagram for the y-axis closed-loop control.

Simulation Results

Using the model described above, the closed-loop system was simulated and the controller tuned in order to provide stability and to reject the disturbances that tend to shift the air gap from its nominal value. During system operation one of the disturbances d_y occurs as a consequence of longitudinal motion of the TLIM secondary. Fig. 9 shows the disturbance d_y signals as well as the transient responses for axis y displacement and current i_{2b}. It can be seen that the AMB has a fine dynamic performance with small deviations of position and current.

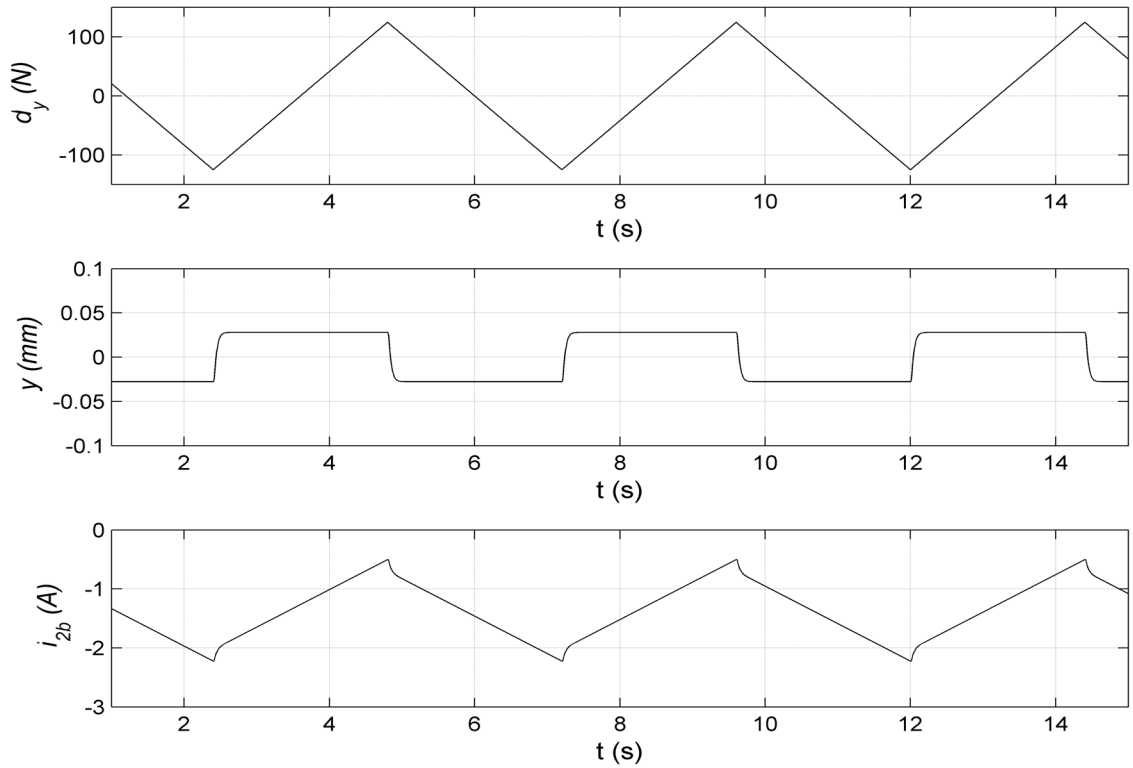

Fig. 9 Transient response along axis y and current i_{2b} due the disturbance d_y.

Experimental Results

To check the behavior of the ABM control system, several tests were performed. Two of them are presented in what follows.

With the MATÆOS turned off, the AMB was initially in steady-state at the equilibrium point given by x = 0.1mm and y = -0.4mm. Notice that due to calibration offsets of the sensors, these values, which correspond closely to the secondary centered with respect to the motor primary and AMB stator, are nonzero.

A longitudinal motion was manually imposed to the TLIM secondary. In this way the disturbance d_y is simulated. Fig. 10 shows the radial deviations along x (black) and y (red) as functions of time; currents i_{2a} (black) and i_{2b} (red) are shown in Fig. 11.

The results show that the control system rejected the disturbance induced by the secondary longitudinal motions. As expected, the deviations observed for both axes were smaller than 0.2mm and the currents did not reach their maximum admissible values.

In the second test with the MATÆOS turned off, the AMB was initially in steady-state at the equilibrium point given by x = -0.1mm and y = -0.4mm. The motor was turned on at time 1.4 sec and it remained so until time 15.4 sec, when it was turned off. Fig. 12 shows the radial deviations along x (black) and y (red) as functions of time; currents i_{2u} (black), i_{2v} (red), and i_{2w} (green) are shown in Fig. 13.

The results show that the control system rejected the disturbance induced by both the secondary longitudinal and radial motions. For each axis it can be noticed that the deviation from the equilibrium point attained its maximum value at the time instants when the velocity of the secondary was reversed and the secondary had its largest length in balance. This event occurred at times 3.8, 8.6 and 13.4 sec. As expected, the deviations observed for both axes were smaller than 0.3mm and the currents did not reach their maximum admissible values.

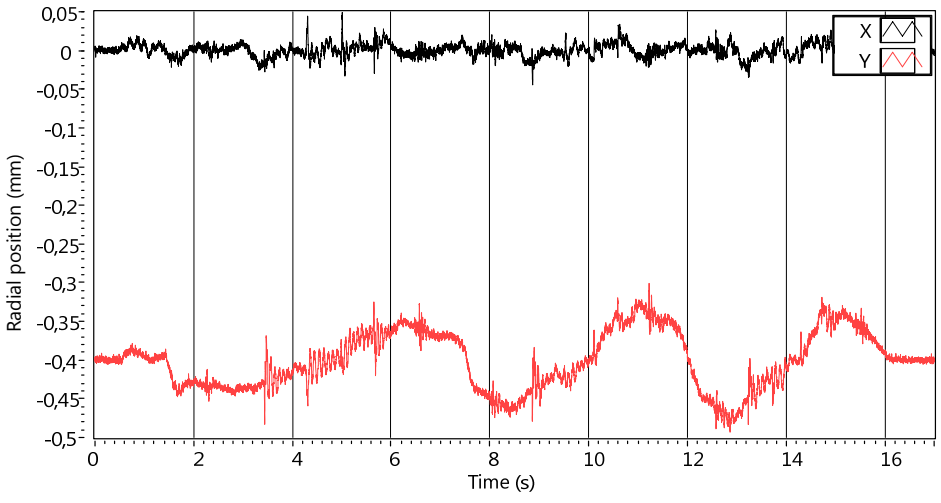

Fig. 10 AMB radial deviations along x and y due the disturbance d_y.

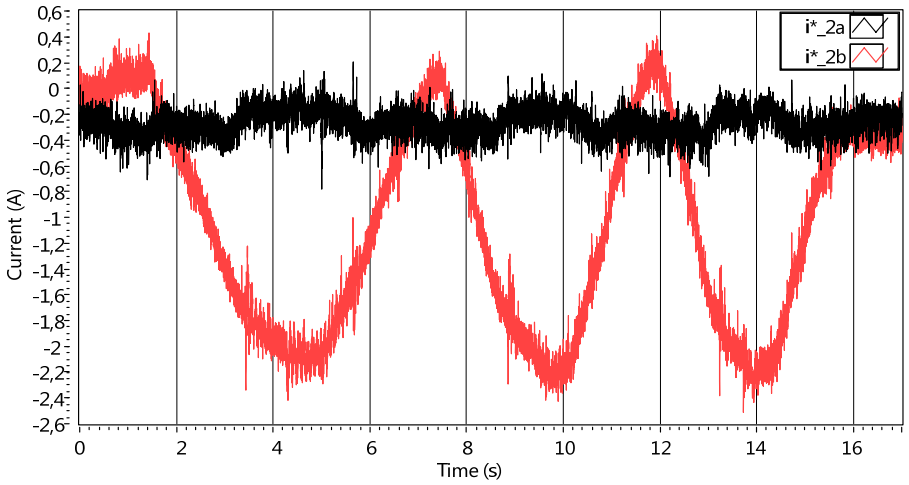

Fig. 11 AMB currents i_{2a} and i_{2b} due the disturbance d_y.

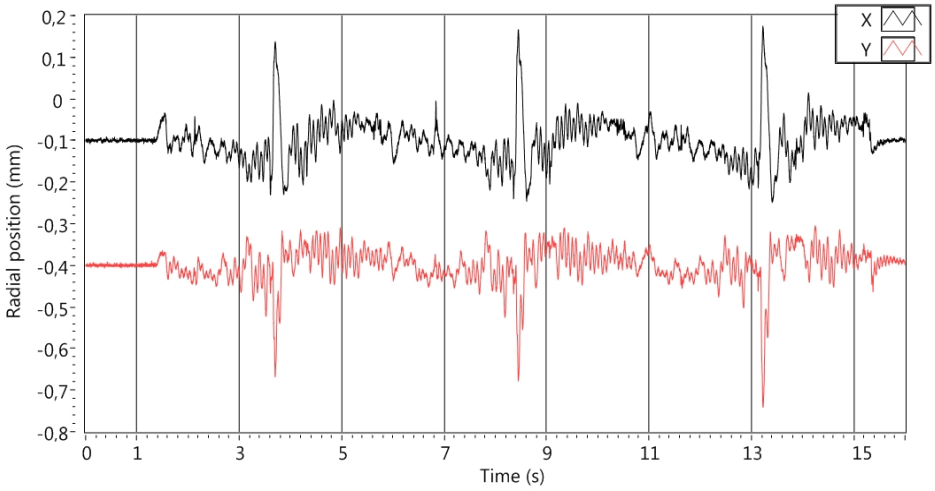

Fig. 12 AMB radial deviations along x and y with motor turned on.

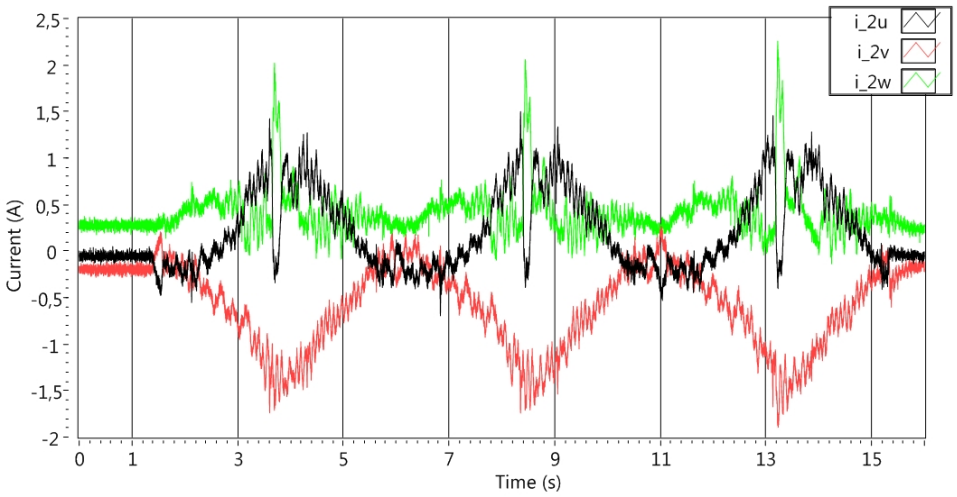

Fig. 13 AMB currents i_{2u}, i_{2v} and i_{2w} with motor turned on.

Conclusions

In this paper an AMB system was proposed to be used in a TLIM intended to be used in onshore oil exploitation with particular emphasis to the experimental results obtained with the prototype in operation. The tests performed showed that the closed-loop system is stable and exhibits a satisfactory transient response. The disturbance has been stronger during the secondary axial motion reversal when a fast dynamical response of the power circuit is required.

The inclusion in the model of both the effect of magnetic force produced by the secondary displacement from the center of the TLIM primary and of the coupling between the force and the bearing displacement seemed to be essential to guarantee the appropriate performance of the AMB.

It is well known that the position sensor can be strongly affected by noise [4]. In this work, where the main sources of noise were the power amplifier of the AMB and the power inverter used to drive the TLIM, this fact was confirmed. Appropriate grounding of these drivers was required to reduce the sensor noise effects.

There are just a few cases of FPGA-based controller implementation for magnetic levitation systems reported in the literature. Just one reference by the same authors of the present paper has been found focusing on the application of AMBs to TLIMs [6]. This article aims to be a contribution in both topics.

In the next step of this research the mechanical bearing of the prototype will be replaced by an AMB.

References

[1] B. P. Alvarenga, A proposal of application of a tubular linear induction motor for oil extraction, PhD thesis, Polytechnic School of USP, 2004 (in Portuguese).

[2] W. M. Rossini, B. P. Alvarenga, I. E. Chabu, J. J. Cruz, J. R. Cardoso, R. M. Sales, “New concept for lifting in Oil Wells”. IEEE Transactions on Industry Applications, v.44, n.4, p. 951-961, July/August, 2008.

[3] M. E. F. Kasarda, **“**An Overview of Active Magnetic Bearing Technology and Applications”. The Shock and Vibrations Digest, 2000, p. 225-231.

[4] G. Schweitzer, E. H. Maslen, Magnetic Bearings: theory, design, and applications to rotating machinery, London – New York: Springer Verlag, 2009.

[5] A. Chiba, T. Fukao, O. Ichikawa, M. Oshima, M. Takemoto and D.G. Dorrell, Magnetic Bearings and Bearingless Drives. Boston: Elsevier Newnes Press, 2005.

[6] E. A. Costa, I. E. Chabu, J. J. Cruz, **“**Application of active magnetic bearing for tubular linear induction motor in oil pumping”. Proceedings 11th International symposium on magnetic bearings**,** Nara, Japan, August 26-29, 2008, p. 225-231.

[7] E. A. Costa, Active magnetic bearing applied to a tubular linear induction motor, PhD thesis, Polytechnic School of USP, 2009 (in Portuguese).